INL/CON-24-76616-Revision-0

Kinetic Plasma Simulation in the MOOSE Framework: Verification of Electrostatic Particle In Cell Capabilities

October 2024

Grayson S Gall, Amanda M Lietz, Derek R Gaston, Pierre-Clement A Simon, Casey T Icenhour, Logan H Harbour

Changing the World's Energy Future

INL is a U.S. Department of Energy National Laboratory operated by Battelle Energy Alliance, LLC

INL/CON-24-76616-Revision-0

Kinetic Plasma Simulation in the MOOSE Framework: Verification of Electrostatic Particle In Cell Capabilities

Grayson S Gall, Amanda M Lietz, Derek R Gaston, Pierre-Clement A Simon, Casey T Icenhour, Logan H Harbour

October 2024

Idaho National Laboratory
Idaho Falls, Idaho 83415

http://www.inl.gov

Prepared for the
U.S. Department of Energy
Under DOE Idaho Operations Office
Contract DE-AC07-05ID14517

Kinetic Plasma Simulation in the MOOSE Framework: Verification of Electrostatic Particle In Cell Capabilities

Grayson S. Gall [1,*], Logan H. Harbour[2], Casey T. Icenhour[2], Pierre-Clément A. Simon[2], Derek Gaston[2], Amanda M. Lietz[1]

[1]North Carolina State University, Raleigh, North Carolina; [2]Idaho National Laboratory, Idaho Falls, Idaho

[leave space for DOI, which will be inserted by ANS]

ABSTRACT

In magnetic confinement nuclear fusion reactors, the interaction between the plasma edge and plasma facing components is extremely important. At the plasma edge, a kinetic representation such as particle-in-cell (rather than a fluid representation) is required to accurately capture the plasma behavior. General purpose particle-in-cell plasma simulation capabilities have been developed in the Multiphysics Object-Oriented Simulation Environment (MOOSE) framework. This new capability is a part of the development of a new MOOSE-based framework for modeling plasma facing components, the Fusion ENergy Integrated multiphys-X (FENIX) framework. In this work, the verification of foundational particle-in-cell capabilities in FENIX is presented. This new plasma simulation capability has three main components: moving particles in discrete steps on the finite element mesh, mapping charge density from the particle's location to the finite element mesh, and solving for the electrostatic potential based on the charge density mapped from particles to the mesh. In this paper, simple verification problems demonstrating each of these new capabilities are presented, and future work includes electromagnetic capabilities and Monte Carlo collisions with neutral gas particles.

Keywords: Particle In Cell, Plasma, Computational Fusion, MOOSE, FENIX

1. INTRODUCTION

As fusion energy technology has developed in recent years, more attention must be given to the engineering challenges of a realistic power plant [1]. Plasma facing components (PFCs) in fusion devices require significant development before the technology can provide energy to the grid. The prohibitive resource requirements for fusion experiments to generate data on the conditions that PFCs experience are scarce and difficult to obtain. Thus, there is a need for a multiphysics framework that can capture the behavior of PFCs in these conditions. The Fusion Energy Sciences Advisory Committee has identified a need for computational tools to study these systems [1]. To meet this need, the Fusion ENergy Integrated multiphys-X (FENIX) framework [2] is being built on the Multiphysics Object-Oriented Simulation Environment (MOOSE) framework [3]. While other tools have been developed to model important aspects of PFCs [4, 5, 6] FENIX will take advantage of the modularity of MOOSE's native multiphysics coupling and will be the first fully open source tool capable of accurately modeling PFCs. FENIX aims to combine existing MOOSE modules, such as heat conduction, thermomechanics, and thermal hydraulics, and couple them with the MOOSE-based applications Cardinal [7, 8] and the Tritium Migration Analysis Program, version

*gsgall@ncsu.edu

8 (TMAP8) [9, 10] to accurately model PFCs [2]. A key part of developing this framework is kinetic plasma simulation capability using a particle-in-cell (PIC) scheme, which we discuss in this paper. Three key capabilities that have been verified are movement of the particles in discrete steps over time, the ability to map charge from particles in space to the finite element mesh, and using the charge mapped from the particles to finite element mesh as input required to solve Poisson's equation for the electrostatic potential. The particle motion leverages MOOSE's ray-tracing module [11], and the mapping of charge from particles to the finite element mesh utilizes functionality available through libMesh. In Section 2, the particle pushing scheme used for electromagnetic PIC simulations is discussed in detail, and several verification cases are presented. Charge mapping from the particles to the finite element mesh is discussed in Section 3, and two examples of this functionality are presented. Additionally, an example of solving Poisson's equation based on a charge density mapped from particles to the finite element mesh is presented. Ongoing development efforts and future plans for this new capability are presented in Section 4.

2. PARTICLE PUSH

In PIC simulations, the standard approach for moving charged particles through electromagnetic forces is to use a leap frog method. A leap frog method in this context is one in which the velocity of the particle and position of the particle are updated at different times, offset by one-half time step. In FENIX, the position of the particle, $\vec{r}$, is always advanced using a full-time step. The particle velocity, $\vec{v}$, however, is updated using a half time step on the first time step, and on subsequent steps, the velocity is advanced using a full time step. This results in the particle velocity being calculated with a one-half time step offset from the position of the particle. This scheme is visualized in Figure 1.

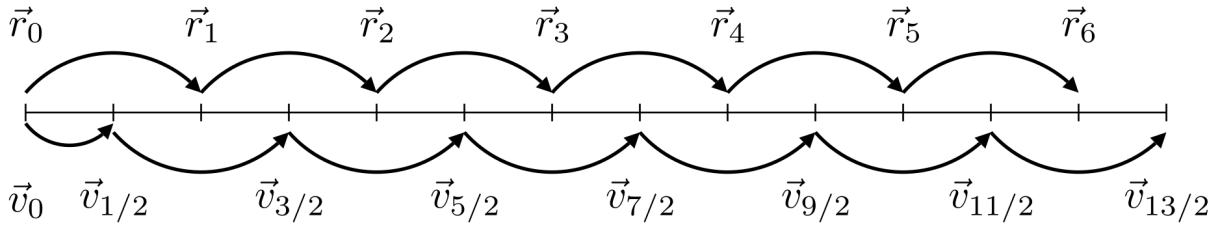

Figure 1. Visualization of the update scheme used in a leap frog method. The particle position, $\vec{r}$, is updated at whole time steps, and the particle velocity, $\vec{v}$, is updated with a one-half time step offset.

In magnetized (or electromagnetic) PIC simulations, the de facto standard particle stepping algorithm is commonly known as the Boris algorithm [12, 13, 14]. This algorithm is similar to a leap frog method and has second order accuracy in time when solving the equations of motion for a charged particle, given by

$$\frac{d\vec{r}}{dt} = \vec{v} \tag{1}$$

and

$$\frac{d\vec{v}}{dt} = \frac{q}{m}\left[\vec{E} + \vec{v} \times \vec{B}\right] \tag{2}$$

where q is the particle's charge, m is the particle's mass, and $\vec{E}$ and $\vec{B}$ are the electric and magnetic fields that the particle is subject to, respectively.

In the Boris algorithm, Equations (1) and (2) are discretized with a central difference scheme and the acceleration due to the electric field and magnetic field are separated. First, half of the impulse due to the electric field is applied to the particle, as

$$\vec{v}^{\,-} = \vec{v}_n + \frac{q}{m}\vec{E}_n\frac{\Delta t}{2} \tag{3}$$

where $\vec{v}^{\,-}$ is an intermediate particle velocity, $\vec{v}_n$ is the particle velocity at step n, and $\vec{E}_n$ is the electric field at step n. The velocity of the particle after rotation due to the magnetic field is derived as

$$\vec{v}^{\,+} = \vec{v}^{\,-} + \vec{v}^{\,\prime} \times \vec{s}, \tag{4}$$

with

$$\vec{v}^{\,\prime} = \vec{v}^{\,-} + \vec{v}^{\,-} \times \vec{l} \tag{5}$$

where

$$\vec{l} = \frac{q}{m}\vec{B}_n\Delta t, \tag{6}$$

which accounts for the effect of $\vec{B}_n$, the magnetic field at step n. $\vec{s}$ is defined as

$$\vec{s} = \frac{2\vec{l}}{1 + \vec{l}\cdot\vec{l}}. \tag{7}$$

Finally, the rotation due to the presence of the magnetic field is then applied with

$$\frac{\vec{v}^{\,+} - \vec{v}^{\,-}}{\Delta t} = \frac{q}{m}\left(\vec{v}^{\,+} + \vec{v}^{\,-}\right) \times \vec{B}_n, \tag{8}$$

and the final impulse due to the electric field is then applied to the particle using

$$\vec{v}_{n+1} = \vec{v}^{\,+} + \frac{q}{m}\vec{E}_n\frac{\Delta t}{2}. \tag{9}$$

The implementation of the Boris algorithm was verified using several single particle motion tests: constant electric field, cyclotron motion, and $\vec{E} \times \vec{B}$ drift motion.

2.1. Constant Electric Field

When subject to a constant electric field, and in the absence of a magnetic field, the Boris algorithm can replicate the analytic solution for single particle motion exactly, up to machine precision [15]. In order to verify that the implementation in FENIX can replicate this result, a single particle was subject to a constant electric field that replicates projectile motion. A single particle of mass, $m = 1$ [kg], with charge, $q = 1$ [C], was subjected to an electric field given by

$$\vec{E} = -9.81\hat{y}\left[\frac{\mathrm{V}}{\mathrm{m}}\right] \tag{10}$$

with initial velocity conditions given by

$$v_x(0) = v_y(0) = 10\left[\frac{\mathrm{m}}{\mathrm{s}}\right] \tag{11}$$

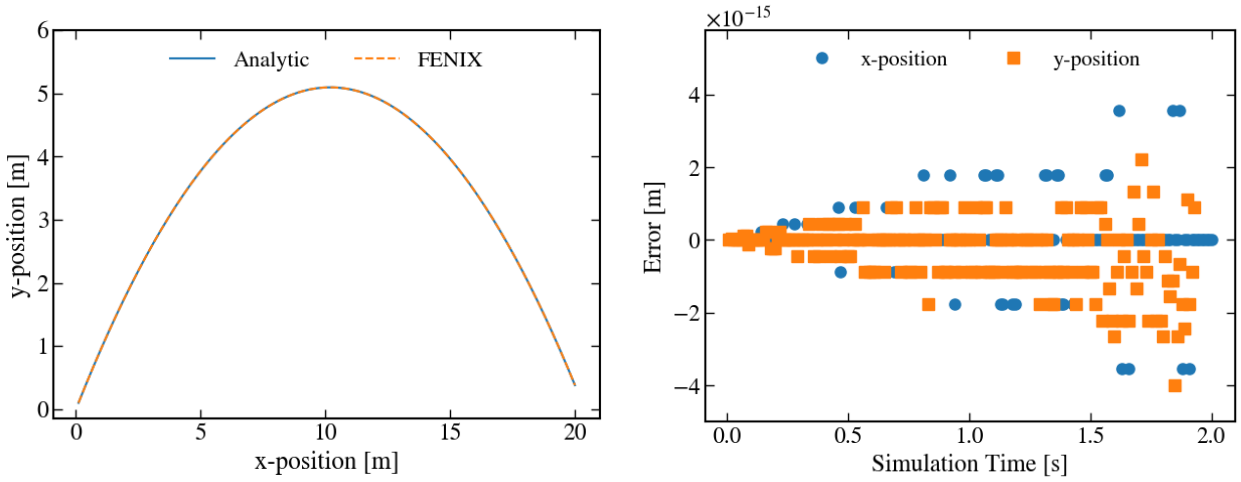

(a) **(b)**

Figure 2. Verification of FENIX's predictions for the path of a single particle in a constant electric field. (a) shows the comparison between the FENIX solution for the path of a single particle and the analytic solution for the single particle motion. (b) shows the error in the FENIX solution.

where $v_x(0)$ and $v_y(0)$ are the x and y velocities of the particle at time $t = 0$, respectively.

The path of the single particle as computed with FENIX is compared with the path from the analytic solution in Figure 2a. The error in FENIX's solution was then calculated by simply taking the difference between the analytic solution and the FENIX solution for the particle's path, this error is visualized in Figure 2b. The greatest error in the FENIX solution for the particle's path is on the order of machine precision. This precision is expected and provides evidence that the Boris algorithm has been properly implemented.

2.2. Cyclotron Motion

In the presence of a constant magnetic field, a single charged particle will orbit in a circle in a plane normal to the magnetic field. The constant magnetic field used for this test is given by

$$\vec{B} = 1\,\hat{z}\ \ [\mathrm{T}]\,. \tag{12}$$

The path of a particle in the presence of a constant magnetic field is given by

$$x(t) = r_L \sin(\omega_c t) \tag{13}$$

and

$$y(t) = r_L \cos(\omega_c t) \tag{14}$$

where

$$r_L = \frac{v_\perp}{\omega_c} \tag{15}$$

and

$$\omega_c = \frac{q\vec{B}}{m} \tag{16}$$

and $v_\perp$ is the magnitude of the particle velocity in the plane normal to the magnetic field. $v_\perp$ is given by

$$v_\perp = 1\ \left[\frac{\mathrm{m}}{\mathrm{s}}\right]. \tag{17}$$

In this test a particle of mass mass $m = 1$ [kg], and charge $q = 1$ [C] is subjected to the magnetic field given by Equation (12) .

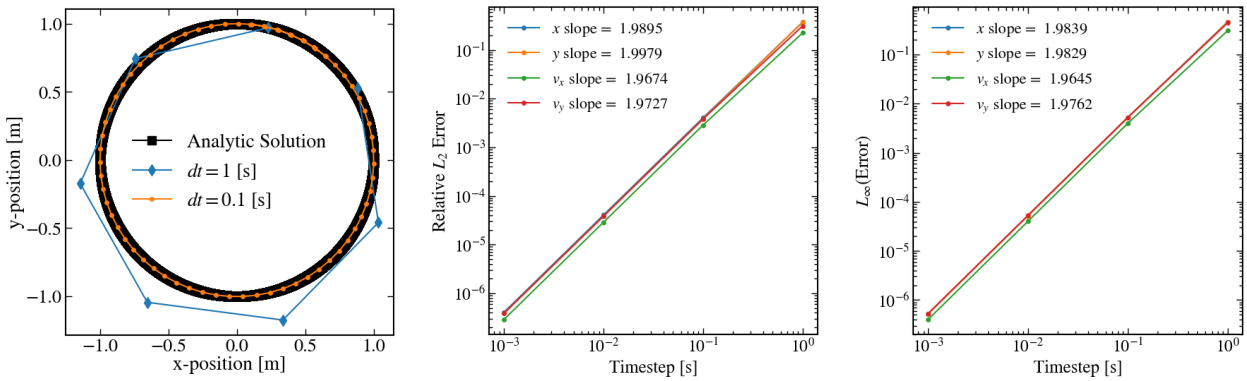

(a) **(b)** **(c)**

Figure 3. Verification of FENIX's predictions for the path of a single particle in a constant magnetic field. (a) shows the comparison between the FENIX solution for the path of a single particle computed with two different time steps and the analytic solution for the single particle motion. (b) shows the L_∞ norm of the error in the FENIX solution as time step decreases. Modeling results converge toward the analytic solution as the time step decreases.

A comparison between the exact analytic solution for cyclotron motion and the FENIX solution was performed and is presented in Figure 3a. Two time steps are used for this comparison 0.1 [s] and 1 [s]. Additionally, the FENIX solution using a time step of 1 [s] demonstrates an important feature of the Boris algorithm. This feature is that the Boris algorithm provides a global bound on energy error resulting in a path that while inaccurate is not completely unrealistic. The two different time steps shown in Figure 3a were selected to demonstrate the convergence of the solution to the analytic solution. The particle's path calculated with smaller times steps is not shown in Figure 3a, because including them would obscure the visibility of the analytic solution. However, the relative L_2 norm of the error and the L_∞ norm of the error for all time steps are visualized in figures 3b and 3c respectively. A line was fit to the logarithm of the error in order to determine the order of convergence. The slope of lines in figures 3b and 3c represent the order of convergence in time. As expected, the Boris algorithm demonstrates second order convergence in time.

2.3. $\vec{\mathbf{E}} \times \vec{\mathbf{B}}$ Drift

A more complex particle motion is that of the so-called $\vec{E} \times \vec{B}$ drift. When subject to perpendicular electric and magnetic fields, the path a charged particle takes will have a characteristic rotation similar to that of cyclotron motion discussed in Section 2.2 with an additional guiding center drift. In the result presented in Figure 4, a single particle of charge $q = 1$ [C] and mass $m = 1$ [kg] is subject to a constant electric field given by

$$\vec{E} = 0.05\,\hat{x}\,\left[\frac{\mathrm{V}}{\mathrm{m}}\right] \tag{18}$$

and a perpendicular constant magnetic field given by

$$\vec{B} = 1\,\hat{z}\ [\mathrm{T}]\,. \tag{19}$$

An exact analytic solution for the particle path in this configuration is not available. Instead, an approximate

solution for the path of a single charged particle subject to a perpendicular electric and magnetic field is given by

$$x(t) \approx r_L \sin(\omega_c t) \tag{20}$$

and

$$y(t) \approx r_L \cos(\omega_c t) - \frac{E_x}{B_z} t. \tag{21}$$

More detail on the derivation of this approximate solution is available in [16, 17].

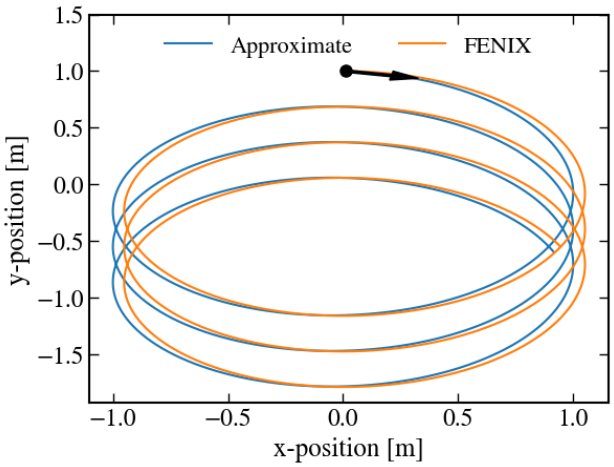

Figure 4. Comparison between the FENIX solution and the approximate theoretical solution for the $\vec{E} \times \vec{B}$ drift of a single charged particle. Where the black dot represents the initial particle position and the arrow represents the direction in which the particles are traveling

The FENIX solution shown in Figure 4 agrees well with the approximate theoretical solution in that it demonstrates the processing cyclotron and drifting motion that should be expected for this field configuration.

3. CHARGE MAPPING

In FENIX, like in other finite element PIC codes [15, 18], the charge density is defined at the nodes of the finite element mesh. The finite element basis functions are used to map charge from particles to the finite element mesh. If each computational particle is treated as a point particle in space, then the charge density can be approximated as

$$\rho(\vec{r}) \approx \sum_{j=1}^{N} q_j \delta(\vec{r} - \vec{r}_j) \tag{22}$$

where q_j is the charge of the j^{th} particle, $\vec{r}_j$ is the position of the j^{th} particle, and N is the total number of particles in the system. In the finite element representation of Poisson's equation, knowledge of the charge density *alone* is not required. Instead, knowledge of the *inner product* of the charge density and the i^{th} basis function, ϕ_i, is required. This quantity is given by

$$\langle \rho(x), \phi_i(x) \rangle = \sum_{j=1}^{N_i} q_j \phi(\vec{r} - \vec{r}_j) \tag{23}$$

where N_i is the number of particles in the region where the i^{th} basis function is non-zero [18].

It is important to note that this does not give direct knowledge of the charge density at each node. However, this representation yields an efficient method for solving Poisson's equation with charge mapping that is similar to the cloud-in-cell representation presented by Birdsall and Langdon [13]. Two simple verification tests of this new capability were completed. The first was a one-dimensional charge mapping from a single computational particle located at the point $x = 0.5$ [m], with a charge of $q = 1$ [C], to a finite element mesh with four nodes. The expected charge mapping from this setup is that each of the closest two nodes to the computational particle should have a charge of $q_i = 0.5$ [C] each. This result can be seen in Figure 5a. To ensure that this capability generalizes to higher dimensions correctly, a two-dimensional version of the test was performed. In this scenario, the charge of the particle is the same, but now it is located at the point $\vec{r} = (0.5, 0.5)$ [m]. The mesh was constructed to have 16 evenly spaces nodes on the domain $x \in [0, 1]$ and $y \in [0, 1]$. In this scenario, the expected result is that each of the four closest nodes to the particle should have a charge of $q_i = 0.25$ [C]. This result can be seen in Figure 5b.

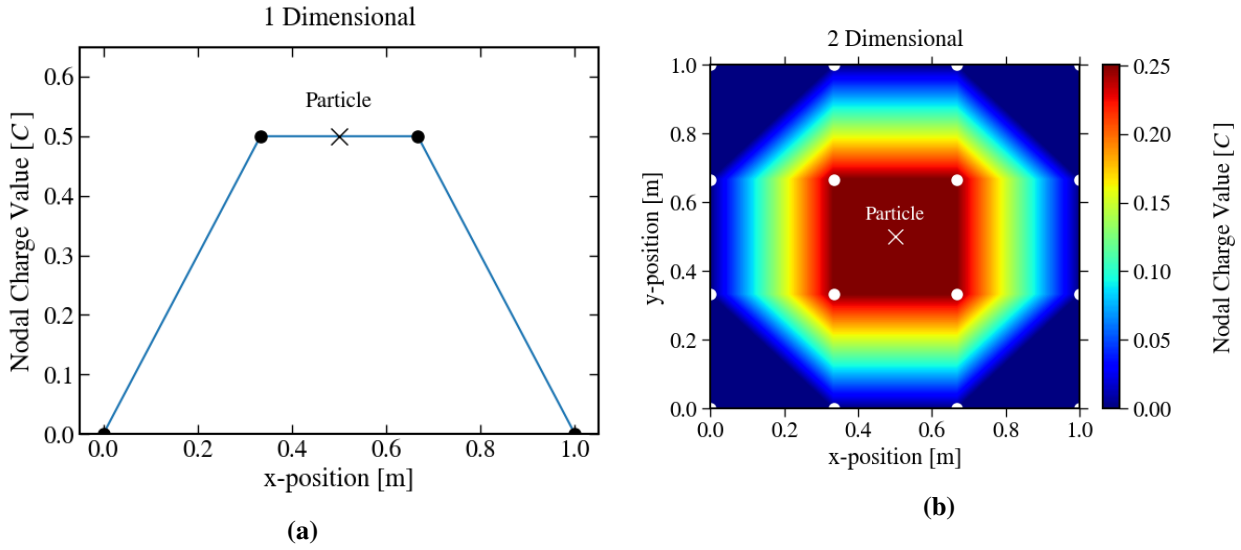

Figure 5. Charge mapping demonstrations in (a) 1D and in (b) 2D. Black dots in (a) and white dots in (b) represent the nodes of the finite element mesh. The X marks the position of the particle.

3.1. Electrostatic Potential Solve

Poisson's equation can be used to solve for the electric field given a charge density and is given by

$$-\nabla^2 \phi = \frac{\rho}{\varepsilon_0}. \tag{24}$$

The electric field is not directly calculated; rather, the electrostatic potential is determined based on the charge density and can be used to calculate the electric field. In order to verify the implementation of charge mapping and subsequently solving for the electrostatic potential, a simple test was performed in FENIX. A simple potential was selected and is given by

$$\phi = x(1 - x) \ \text{[V]}\,. \tag{25}$$

Based on the potential, the corresponding charge density was calculated to be

$$\frac{\rho}{\varepsilon_0} = 2 \left[\frac{\mathrm{V}}{\mathrm{m}^2} \right]. \tag{26}$$

A one-dimensional mesh with five nodes on the domain $x \in [0, 1]$ was used, and two macro particles of charge $q = 1$ [C] were placed at each node giving the required uniform charge density, Equation (26). The potential was then solved using existing MOOSE kernels. Dirichlet boundary conditions,

$$\phi(0) = \phi(1) = 0, \tag{27}$$

were also used during the finite element solve.

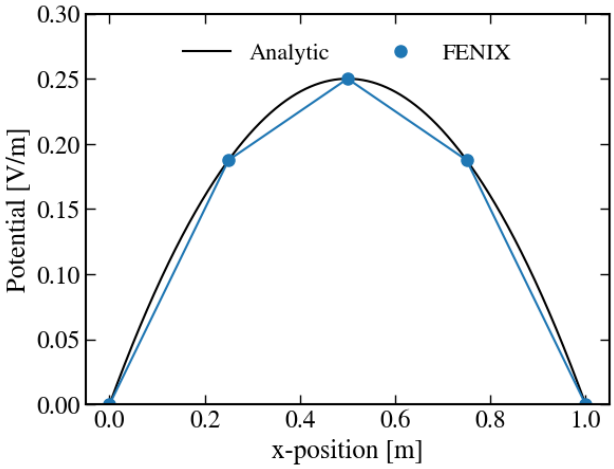

Figure 6. Comparison between the analytic solution for the electrostatic potential and the resulting FENIX solution using the charge density mapped from particles. Dots in the electrostatic potential are the location of the nodes of the finite element mesh.

The agreement between the analytic solution and the FENIX solution at the nodes, seen in Figure 6, of the finite element mesh demonstrates that charge mapping and the subsequent potential solve capabilities have been implemented correctly.

4. FUTURE WORK

The next steps for verification will be to demonstrate that FENIX can reproduce two well-known kinetic plasma effects: Landau damping and the two-stream instability [16, 17]. Additionally, recent work has provided an analytic solution for a collisionless single species plasma, which will be replicated using FENIX [19]. We plan to replicate the result presented in [19] before moving onto adding support for Monte Carlo collisions. After these verification tests are performed, the MOOSE electromagnetics module [20] will be coupled to FENIX, and Monte Carlo collision capabilities will be developed.

5. CONCLUSIONS

Verification for the foundational capabilities required for kinetic plasma simulations has been completed for the MOOSE application FENIX. Several cases of single particle motion have shown that the Boris algorithm

for particle stepping has been implemented correctly and has second order accuracy in time. The charge mapping examples demonstrate that first order charge mapping from particles to the finite element mesh has been implemented correctly. Finally, a charge density was supplied by mapping charge from particles to the finite element mesh, and Poisson's equation was solved using existing MOOSE infrastructure. The sum of this work demonstrates that the foundational infrastructure required for collisionless electrostatic kinetic plasma simulation has been implemented correctly. The new capabilities presented in this work give the developers confidence that the new capabilities are implemented correctly and that the capability required for modeling PFCs simulations will be built on a solid foundation.

ACKNOWLEDGEMENTS

This work was supported through the INL Laboratory Directed Research & Development (LDRD) Program under DOE Idaho Operations Office Contract DE-AC07-05ID14517. This manuscript has been authored by Battelle Energy Alliance, LLC under Contract No. DE-AC07-05ID14517 with the U.S. Department of Energy. The United States Government retains and the publisher, by accepting the article for publication, acknowledges that the United States Government retains a nonexclusive, paid-up, irrevocable, world-wide license to publish or reproduce the published form of this manuscript, or allow others to do so, for United States Government purposes.

This research made use of Idaho National Laboratory's High Performance Computing systems located at the Collaborative Computing Center and supported by the Office of Nuclear Energy of the U.S. Department of Energy and the Nuclear Science User Facilities under Contract No. DE-AC07-05ID14517.

REFERENCES

[1] Fusion Energy Sciences Advisory Committee (FESAC). "Powering the Future, Fusion & Plasmas." Technical report, U.S. Department of Energy, Office of Science, Fusion Energy Science (2022).

[2] P.-C. A. Simon, C. T. Icenhour, M. Shimada, A. Lindsay, G. Giudicelli, L. Harbour, D. Gaston, H. Brooks, A. J. Novak, M. Eltawila, A. M. Lietz, and G. Gall. "Developing Multiphysics, Integrated, High-Fidelity, Massively Parallel Computational Capabilities for Fusion Applications Using MOOSE." In *Proceedings of the Pacific Basin Nuclear Conference 2024*. Idaho Falls, ID (2024).

[3] A. D. Lindsay, D. R. Gaston, C. J. Permann, J. M. Miller, D. Andrš, A. E. Slaughter, F. Kong, J. Hansel, R. W. Carlsen, C. Icenhour, L. Harbour, G. L. Giudicelli, R. H. Stogner, P. German, J. Badger, S. Biswas, L. Chapuis, C. Green, J. Hales, T. Hu, W. Jiang, Y. S. Jung, C. Matthews, Y. Miao, A. Novak, J. W. Peterson, Z. M. Prince, A. Rovinelli, S. Schunert, D. Schwen, B. W. Spencer, S. Veeraraghavan, A. Recuero, D. Yushu, Y. Wang, A. Wilkins, and C. Wong. "2.0 - MOOSE: Enabling massively parallel multiphysics simulation." *SoftwareX*, **volume 20**, p. 101202 (2022).

[4] J. Candy. "AToM (Advanced Tokamak Modeling)." Technical report, General Atomics, San Diego, CA (United States) (2017).

[5] A. Sircar, J. W. Bae, E. Peterson, J. Solberg, and V. Badalasi. "FERMI: A multi-physics simulation environment for fusion reactor blanket." Technical report, Lawrence Livermore National Lab.(LLNL), Livermore, CA (United States) (2022).

[6] X. Bonnin, W. Dekeyser, R. Pitts, D. Coster, S. Voskoboynikov, and S. Wiesen. "Presentation of the New SOLPS-ITER Code Package for." *Plasma and Fusion Research*, **volume 11**(Specialissue1), pp. 1–6 (2016).

[7] A. Novak, D. Andrs, P. Shriwise, J. Fang, H. Yuan, D. Shaver, E. Merzari, P. Romano, and R. Martineau. "Coupled Monte Carlo and Thermal-Fluid Modeling of High Temperature Gas Reactors Using Cardinal." *Annals of Nuclear Energy*, **volume 177**, p. 109310 (2022).

[8] M. Eltawila et al. "Investigation of CAD-based Geometry Workflows for Multiphysics Fusion Problems Using OpenMC and MOOSE." In *Proceedings of the Pacific Basin Nuclear Conference (PBNC)*. American Nuclear Society, Idaho Falls, ID (2024). Submitted.

[9] P.-C. A. Simon, P. W. Humrickhouse, and A. D. Lindsay. "Tritium Transport Modeling at the Pore Scale in Ceramic Breeder Materials Using TMAP8." *IEEE Transactions on Plasma Science*, pp. 1–7 (2022).

[10] A. D. Lindsay, C. T. Icenhour, P.-C. A. Simon, and G. Singh. "idaholab/TMAP8." (2021). URL https://github.com/idaholab/TMAP8.

[11] L. Harbour. "Ray Tracing Module." URL https://mooseframework.inl.gov/modules/ray_tracing/index.html.

[12] J. P. Boris et al. "Relativistic plasma simulation-optimization of a hybrid code." In *Proc. Fourth Conf. Num. Sim. Plasmas*, pp. 3–67 (1970).

[13] C. K. Birdsall and A. B. Langdon. *Plasma physics via computer simulation*. Adam Hilger (1991).

[14] H. Qin, S. Zhang, J. Xiao, J. Liu, Y. Sun, and W. M. Tang. "Why is Boris algorithm so good?" *Physics of Plasmas*, **volume 20**(8) (2013).

[15] Z. Eckert, J. J. Boerner, T. H. Hall, J. L. Pacheco, R. Hooper, and A. Grillet. "Benchmark Verification of the Aleph PIC-DSMC Program." (2020). URL https://www.osti.gov/biblio/1834990.

[16] F. F. Chen. *Introduction to plasma physics and Controlled Fusion*. Springer (2018).

[17] M. A. Lieberman and A. J. Lichtenberg. "Principles of plasma discharges and materials processing." *MRS Bulletin*, **volume 30**(12), pp. 899–901 (1994).

[18] M. T. Bettencourt, D. A. Brown, K. L. Cartwright, E. C. Cyr, C. A. Glusa, P. T. Lin, S. G. Moore, D. A. McGregor, R. P. Pawlowski, E. G. Phillips, et al. "EMPIRE-PIC: a performance portable unstructured particle-in-cell code." *Communications in Computational Physics*, **volume 30**(SAND-2021-2806J) (2021).

[19] T. Lafleur. "Space-charge affected current flow: an analytical verification solution for kinetic and fluid simulation models." *Plasma Sources Science and Technology*, **volume 31**(11), p. 114008 (2022).

[20] C. T. Icenhour, A. D. Lindsay, C. J. Permann, R. C. Martineau, D. L. Green, and S. C. Shannon. "The MOOSE electromagnetics module." *SoftwareX*, **volume 25**, p. 101621 (2024).